RESPIRATORY MOTION COMPENSATION IN ROTATIONAL ANGIOGRAPHY: GRAPHICAL MODEL-BASED OPTIMIZATION OF AUTO-FOCUS MEASURES

M. Unberath[1,2]*, O. Taubmann*[1,2]*, B. Bier*[1]*, T. Geimer*[1,2]*, M. Hell*[3]*, S. Achenbach*[3]*, A. Maier* [1,2]

[1] Pattern Recognition Lab, Friedrich-Alexander-University Erlangen-Nuremberg
[2] Erlangen Graduate School in Advanced Optical Technologies (SAOT), Germany
[3] Department of Cardiology, Friedrich-Alexander-University Erlangen-Nuremberg

ABSTRACT

Non-recurrent intra-scan motion, such as respiration, corrupts rotational coronary angiography acquisitions and inhibits uncompensated 3D reconstruction. Therefore, state-of-the-art algorithms that rely on 3D/2D registration of initial reconstructions to the projection data are unfavorable as prior models of sufficient quality cannot be obtained. To overcome this limitation, we propose a compensation method that optimizes a task-based autofocus measure using graphical model-based optimization.

The proposed algorithm is validated on two numerical phantom data sets and a clinical scan. In the phantom studies, we found a reduction of the root-mean-square error between the true and estimated motion pattern of $82 \pm 2\,\%$ when the proposed method was used, yielding residual errors well below the voxel size. For the clinical data set, we observed a substantially increased amount of voxels with low reprojection errors indicating superior image quality.

Our results are promising and suggest that the proposed method effectively handles non-recurrent motion while overcoming the need for prior reconstructions.

Index Terms— Cone-beam CT, Markov random fields, Angiography, Cardiac imaging, Discrete optimization

1. INTRODUCTION

C-arm cone-beam CT angiography is the gold standard imaging protocol for diagnostic assessment of cardiovascular disease [1, 2]. Due to the complex structure of the coronary artery tree, multiple projections from selected viewing directions must be acquired to mitigate the effects of projective simplification, such as overlap and foreshortening [3, 4]. The aforementioned problems can be addressed by providing physicians with the 3D anatomy that is reconstructed from rotational angiography [2, 4].

Unfortunately, straight forward reconstruction in a filtered-backprojection sense [5] is impossible. Projection data is acquired over multiple seconds and, thus, corrupted by cardiac and respiratory motion. While phase binning strategies, such as ECG-gating, are effective for cardiac motion [3, 4], they cannot be applied for respiratory motion management. The reason is that respiration is low frequency and, therefore, virtually non-periodic in this context. This is particularly problematic as most currently known methods require a 3D model of the artery centerlines to enable 3D/2D registration. The 3D model is either obtained from a prior scan [6] or from an initial, uncompensated reconstruction [3, 7, 8]. In the general case, however, prior scans are not available and corruption by respiratory motion is substantial, such that initial reconstruction is impossible.

Addressing respiratory motion compensation without assuming that the uncompensated data allows for meaningful reconstruction is much harder and reveals a trade-off between required preconditions and complexity of the estimated motion model. Methods that operate in projection domain directly are known [9] but are currently limited to detector domain shifts parallel to the rotation axis. In this paper we show that graphical model-based optimization of a task-specific autofocus measure allows for the estimation of 3D translations that compensate non-periodic intra-scan respiratory motion. The proposed approach is validated using a numeric 3D vessel centerline phantom adapted from [10] that is augmented to 4D using motion patterns based on [11]. Finally, we demonstrate the applicability of the method to clinical data.

2. MATERIAL AND METHODS

We describe an algorithm for respiratory motion compensation in rotational angiography. To this end, we optimize a task-based autofocus measure using α-expansion moves and graph-cuts. To allow for sparse sampling of the projection sequence, we parametrize the motion model using B-splines rather than a sequence of translation vectors.

2.1. Autofocus measure

Recently, motion compensation algorithms based on image sharpness, i.e. autofocus, measures have received increasing attention [12]. Unfortunately, standard measures are not applicable in the context described here because tomographic reconstruction is infeasible. Reconstruction is restricted to

scenes that are consistent except for the motion that is compensated for. As we opt for respiratory motion compensation, only the four to six images depicting a similar cardiac phase can be considered simultaneously making standard reconstruction impossible. Sparsifying image processing in projection domain, such as vessel centerline extraction, together with modified backprojection operators enable the reconstruction of volumetric potential maps, rather than tomographic images, that serve as cost maps for 3D centerline extraction [13, 14]. Properties of aforementioned potential maps directly relate to the quality of centerline reconstructions and can, therefore, be subject to autofocus measurements.
Assuming that 2D centerlines $\mathcal{T}^{(i)}$ in all views $i = 1, \ldots, N$ corresponding to heart phase c_r are available, we can compute their distance transform as

$$\Gamma^{(i)}(\mathbf{u}) = \Gamma(\mathbf{u}|\mathcal{T}^{(i)}) = d\left(\mathbf{u}, c(\mathbf{u}|\mathcal{T}^{(i)})\right), \tag{1}$$

where $d(\mathbf{u}, \mathbf{v}) = \|\mathbf{u} - \mathbf{v}\|_2$ is the Euclidean distance between image points $\mathbf{u}, \mathbf{v} \in \mathbb{R}^2$ and $c(\mathbf{u}|\mathcal{T}) = \arg\min_{\mathbf{v}\in\mathcal{T}} d(\mathbf{u}, \mathbf{v})$ is the closest point to $\mathbf{u}$ in $\mathcal{T}$. From the distance transforms, the 3D potential map $S_r(\mathbf{x})$ is given by

$$S_r(\mathbf{x}) = \max_i \Gamma^{(i)}(\breve{\mathbf{x}}^{(i)}), \tag{2}$$

where $\breve{\mathbf{x}}^{(i)} \in \mathbb{R}^2$ is the projection of $\mathbf{x} \in \mathbb{R}^3$ onto image plane i. Points exhibiting a very low response S_r are most likely to belong to the 3D centerline, however, they are very sparse as Eq. 2 allows low responses only at positions that consistently project close to the 2D centerlines. For symbolic reconstruction in the sense of 3D minimal-cost-path extraction [13] we favor sharp responses with pronounced local minima and design our auto-focus measure accordingly. It is given by

$$a(S_r) = \left(\sum_{i=1}^{B} g_i \frac{C_i(S_r)}{V_i(S_r)}\right)^{-1}, \tag{3}$$

where $\{V_i, C_i\}$ constitutes the histogram of B bin center values V_i and the respective voxel counts C_i, and g_i is a bin dependent gain that is tuned to emphasize the importance of low-cost bin counts. $a(S_r)$ tends to 0 with increasing numbers of low cost voxels in S_r.

2.2. Motion model, target function, and optimization

It is well known that respiratory motion of the heart can be approximated by a 3D translation [11]. Direct estimation of 3D shifts for every projection requires a cost function that accounts for every image. This, however, is not practical because subsequent images correspond to different heart phases that require separate potential maps which drastically increases the computational demand (see Fig. 1). Consequently, we express the 3D shifts $\mathbf{t}_i \in \mathbb{R}^3$ as a B-spline curve

$$\mathbf{t}_i(\Phi) = \sum_{k=1}^{K} \varphi_k \cdot B_{k,d}(i/N), \tag{4}$$

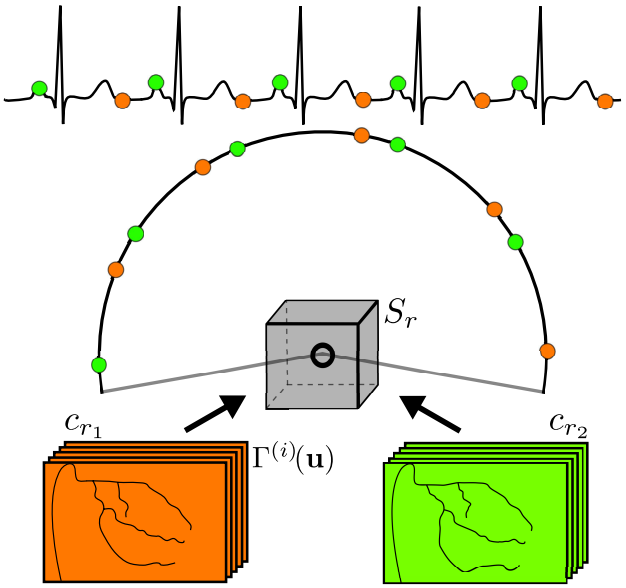

Fig. 1. Images of distinct cardiac phases c_r are scattered over the scan range. Backprojection following Eq. 2 at a specific cardiac phase c_r yields the corresponding potential map S_r.

where $B_{k,d}$ are the B-spline basis functions of degree d and $\Phi = \{\varphi_k \in \mathbb{R}^3 \,|\, k = 1, \ldots, K\}$ is the set of control points, the position of which will be optimized. This approach is advantageous in two ways. First, it yields inherently smooth displacement sequences for all images. Second, a subset of the images, which is defined by the target heart phases selected, suffices for obtaining a global motion trajectory.
Given the motion model we can formulate the target energy function that we seek to minimize. It reads

$$E(\Phi) = \sum_{k=1}^{K} D(\varphi_k|\Phi) + \lambda \sum_{(k,l)\in\mathcal{N}} V(\varphi_k, \varphi_l), \tag{5}$$

where $D(\varphi_k|\Phi)$ enforces data fidelity while $V(\varphi_k, \varphi_l)$ promotes smoothness in neighborhoods $\mathcal{N}$. The data term reads

$$D(\varphi_k|\Phi) = \frac{1}{R}\sum_{r=1}^{R} a\left(S_r \circ T_{(\varphi_k|\Phi)}\right), \tag{6}$$

where $(\varphi_k|\Phi)$ denotes Φ with all elements held constant except for φ_k, $S_r \circ T_\Phi$ is the motion compensated 3D potential map, $T_\Phi(\mathbf{x}, i) = \mathbf{x} + \mathbf{t}_i(\Phi)$, and R is the number of considered heart phases. Moreover, $V(\varphi_k, \varphi_l) = \|\varphi_k - \varphi_l\|_2$ is the Euclidean distance between neighboring control points.
Gradient- and grid search-based optimization of Eq. 5 is, in general, impractical due to the complex shape and high-dimensional domain of the target function, respectively. However, when exchanging continuous control point locations φ_k with discrete candidates $\varphi_k^{(f_k)}$, Eq. 5 takes a form that can be optimized using the α-expansion algorithm [15].

Rather than directly obtaining optimal control point positions that minimize the energy, we recover optimal labels $\mathbf{f} = (f_1, \ldots, f_K)^\top \in \mathbb{N}^K$ that yield shifts $\mathbf{t}(\Phi_\mathbf{f})$, where $\Phi_\mathbf{f} = \{\varphi_k^{(f_k)},\ k = 1, \ldots, K\}$ is the set of control points defined by the current labeling. Put concisely, for all candidate labels $\alpha \in \{1, \ldots, F\}$ we seek to find $\hat{\mathbf{f}}$ such that $\Phi_{\hat{\mathbf{f}}} = \arg\min E(\Phi_{\mathbf{f}'})$, where $\hat{\mathbf{f}}$ is within one α-expansion of the current labeling $\mathbf{f}$. As for particular control points $\varphi_k^{(f_k)}$ the label f_k either changes to α or stays the same, each move is essentially a partitioning problem that is solved using a graph cut. A comprehensive description of the algorithm can be found in [15].

2.3. Experiments

The proposed algorithm is evaluated using two phantom studies and a clinical data set.

For the phantom studies we extract centerlines from an XCAT-based coronary artery phantom [10] and project it using a standard 133 view rotational angiography trajectory and respiratory motion patterns $\mathbf{t}^{\text{gt}}$ derived from [11]. The two simulated acquisitions *Ph1* and *Ph2* comprise a complete and a partial breathing cycle, respectively. Finally, we compare true and estimated motion patterns using the root-mean-square error (RMSE).

For the real data set ground-truth motion is not available and the evaluation is limited to qualitative inspection of the potential maps with and without the proposed motion compensation strategy. Projection domain coronary artery centerlines that are required by the algorithm were extracted using a method similar to [9].

Optimization is applied on multiple scales by increasing the number of both control points and heart phases after convergence, such that $(K, R) \in \{(2,3), (5,3), (7,10)\}$. At the lowest scale, the control points are initialized to yield zero shift. The discrete samples then cover a $4 \times 4 \times 7\,\text{mm}^3$ neighborhood around the starting positions. The potential map has 256^3 voxels with an isotropic size of $0.5\,\text{mm}$.

The bin-dependent gain g_i is selected to heavily favor high counts in low cost histogram bins. It reads

$$g_i = \begin{cases} 10 & \text{if } V_i < 1\,\text{mm}, \\ 1 & \text{if } 1\,\text{mm} \leq V_i < 5\,\text{mm}, \\ 0 & \text{else.} \end{cases} \tag{7}$$

3. RESULTS AND DISCUSSION

The estimated and true shifts of the two phantom data sets are shown in Fig. 2. For *Ph1*, containing a complete respiratory cycle, the RMSE error decreased from $1.5 \pm 0.5\,\text{mm}$ without compensation to $0.29 \pm 0.11\,\text{mm}$ using the proposed method. We observed very similar improvement for *Ph2* comprising the partial cycle, where the RMSE decreased from

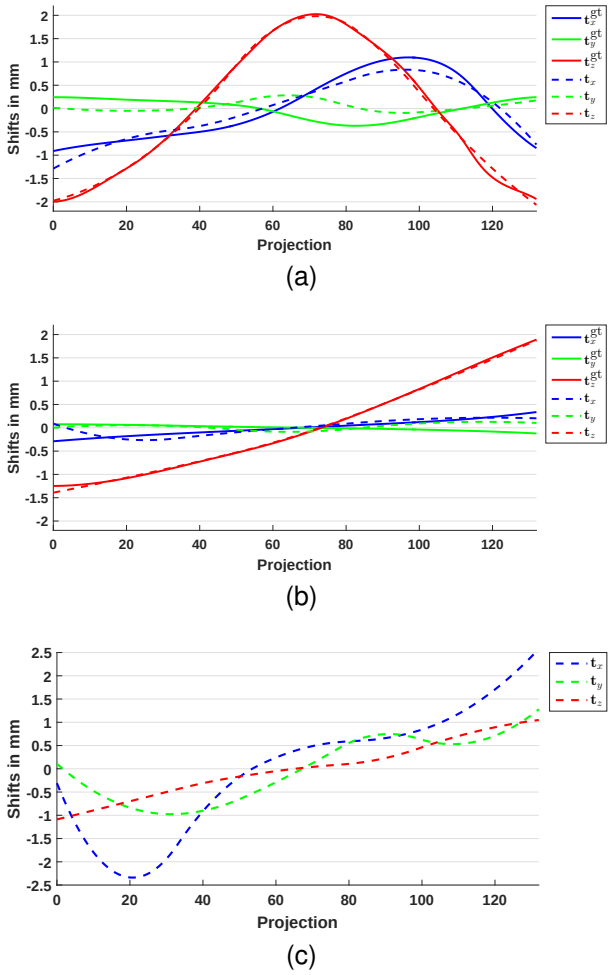

Fig. 2. Estimated and ground-truth motion patterns of *Ph1* and *Ph2* are shown in Fig. 2a and 2b, respectively. Fig. 2c shows the motion pattern estimated for the clinical data set.

$0.85 \pm 0.49\,\text{mm}$ in the uncompensated case to $0.13 \pm 0.07\,\text{mm}$. From Fig. 2 it becomes obvious that compensation works best for the $\mathbf{t}_z$ component. This is not surprising as $\mathbf{t}_z$ accounts for craniocaudal shifts parallel to the rotation axis that are observed over the whole angulation. Estimating motion that occurs in the plane orthogonal to the rotation axis proved more difficult, however, shifts larger than the voxel size of $0.5\,\text{mm}$ were recovered satisfactorily. It is worth mentioning that the residual error in both phantom studies is well below the voxel size of the 3D potential maps.

For the clinical data set, the proposed algorithm yielded the motion pattern shown in Fig. 2c. A volume rendering of the corresponding motion-compensated potential map is shown in Fig. 3b next to the rendering of the respective uncompensated reconstruction. The effect of autofocus-driven motion compensation manifests in substantially more pronounced paths with very low cost that are partly highlighted by green arrows. As potential maps serve as basis for 3D artery center-

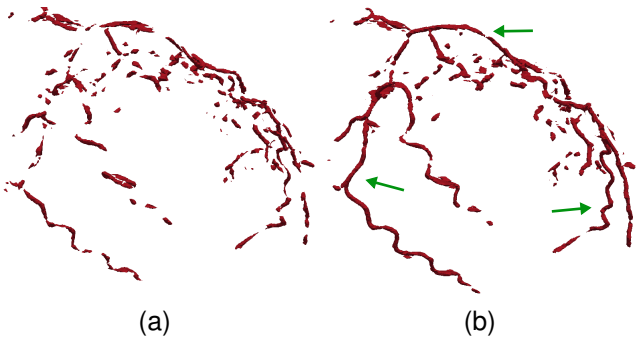

Fig. 3. Fig. 3a and 3b illustrate volume renderings of an uncompensated and a motion-compensated potential map S_r depicting the same cardiac phase, respectively. The window-level is fixed to $[0, 1]$ mm for both renderings.

line extraction [13], the aforementioned improvement directly translates to improved symbolic reconstruction quality.

4. CONCLUSIONS

We proposed 3D translational motion compensation in rotational angiography using graphical model-based optimization of a task-based autofocus measure. The method does not rely on initial reconstructions and, therefore, effectively handles large, non-recurrent motion patterns. We evaluated our approach on two numerical phantom data sets and a clinical acquisition and obtained promising results. Future work will investigate possibilities to improve on motion estimation in the plane orthogonal to the rotation axis.

Acknowledgment

The authors gratefully acknowledge funding of the Erlangen Graduate School in Advanced Optical Technologies (SAOT) in the framework of the German excellence initiative.

5. REFERENCES

[1] C Schwemmer, C Rohkohl, G Lauritsch, K Müller, and J Hornegger, "Residual motion compensation in ECG-gated interventional cardiac vasculature reconstruction.," *Phys. Med. Biol.*, vol. 58, no. 11, pp. 3717–37, 2013.

[2] S Çimen, A Gooya, M Grass, and A F Frangi, "Reconstruction of Coronary Arteries from X-ray Angiography: A Review," *Med. Image Anal.*, vol. 32, pp. 46–68, 2016.

[3] C Blondel, G Malandain, R Vaillant, and N Ayache, "Reconstruction of Coronary Arteries from a Single rotational X-ray projection sequence.," *IEEE Trans. Med. Imaging*, vol. 25, no. 5, pp. 653–663, 2006.

[4] M Unberath, S Achenbach, R Fahrig, and A Maier, "Exhaustive Graph Cut-based Vasculature Reconstruction," in *Proc. ISBI*. 2016, pp. 1143–1146, IEEE.

[5] J Hornegger, A Maier, and M Kowarschik, *CT Image Reconstruction Basics*, pp. 01–09, Alphen aan den Rijn, Netherlands, 1 edition, 2016.

[6] N Baka, B P F Lelieveldt, C Schultz, W Niessen, and T van Walsum, "Respiratory motion estimation in x-ray angiography for improved guidance during coronary interventions.," *Phys. Med. Biol.*, vol. 60, no. 9, pp. 3617–37, 2015.

[7] A Brost, R Liao, N Strobel, and J Hornegger, "Respiratory motion compensation by model-based catheter tracking during EP procedures," *Med. Image Anal.*, vol. 14, no. 5, pp. 695–706, 2010.

[8] G Shechter, C Ozturk, J R Resar, and E R McVeigh, "Respiratory Motion of the Heart From Free Breathing Coronary Angiograms.," *IEEE Trans. Med. Imaging*, vol. 23, no. 8, pp. 1046–56, 2004.

[9] M Unberath, A Aichert, S Achenbach, and A Maier, "Single-frame Subtraction Imaging," in *Proc. CT Meeting*, 2016, pp. 89–92.

[10] C Rohkohl, G Lauritsch, A Keil, and J Hornegger, "CAVAREV - An Open Platform for Evaluating 3D and 4D Cardiac Vasculature Reconstruction," *Phys. Med. Biol.*, vol. 55, no. 10, pp. 2905–2915, 2010.

[11] G Shechter, J R Resar, and E R McVeigh, "Displacement and Velocity of the Coronary Arteries: Cardiac and Respiratory Motion.," *IEEE Trans. Med. Imaging*, vol. 25, no. 3, pp. 369–75, 2006.

[12] A Sisniega, J W Stayman, Q Cao, J Yorkston, J H Siewerdsen, and W Zbijewski, "Motion estimation using a penalized image sharpness criterion for resolution recovery in extremities cone-beam CT," in *Proc. CT Meeting*, 2016, pp. 549–52.

[13] U Jandt, D Schäfer, M Grass, and V Rasche, "Automatic generation of 3D coronary artery centerlines using rotational X-ray angiography.," *Med. Image Anal.*, vol. 13, no. 6, pp. 846–58, 2009.

[14] J Li and L D Cohen, "Reconstruction of 3D tubular structures from cone-beam projections," in *Proc. ISBI*. 2011, pp. 1162–1166, IEEE.

[15] Y Boykov, O Veksler, and R Zabih, "Fast approximate energy minimization via graph cuts," *IEEE Trans. Pattern Anal. Mach. Intell.*, vol. 23, no. 11, pp. 1222–1239, 2001.